



Electrocatalytic properties of Ni–Cu structures fabricated by electrodeposition of Cu on Ni cones

Katarzyna Skibińska¹ · Safya Elsharkawy^{1,2} · Dawid Kutyla¹ · Bożena Boryczko¹ · Mateusz M. Marzec³ · Piotr Żabiński¹

Received: 17 February 2024 / Revised: 25 March 2024 / Accepted: 9 April 2024 / Published online: 29 April 2024
© The Author(s) 2024

Abstract

Ni–Cu alloys are a suitable candidate as a catalyst in Hydrogen Evolution Reaction due to their catalytic performance and good stability. To enhance this activity more, the active surface area of the material should be enhanced. It is commonly achieved by the synthesis of metals and alloys in the form of nanostructures. In this work, Ni cones fabricated by the one-step method were applied as a substrate for the deposition of thin Cu layers. Then, these materials were annealed in an ambient atmosphere to obtain Ni–Cu structures. The investigation of changes in morphology and chemical composition, as well as roughness and wettability before and after the annealing process was performed. Moreover, the measurements of catalytic properties were carried out in 1 M NaOH. The values of the Tafel slope and the electrochemical active surface area were studied. The proposed method can be successfully applied to fabricate structures of other alloys for the desired properties.

Keywords Cones · Ni–Cu alloys · Annealing · Hydrogen evolution reaction · Surface development

1 Introduction

Functional materials are the group of materials that are designed and synthesized for proper function [1]. Desired properties can be achieved by selecting an appropriate fabrication method, which greatly influences the structures and compositions. For example, conical Co catalysts can be prepared by electrochemical deposition in anodic alumina oxide templates or by the one-step method [2]. They are characterized by different morphology, surface evolution and consequently catalytic performance.

Nickel, as a single metal and as a component of alloys, is well known for its catalytic performance in the hydrogen evolution reaction (HER) [3–5]. Electroplating of Ni–Cu alloys has been described in the literature. The structure and

composition of the coatings produced can be influenced by changes in deposition potential [6]. Higher concentrations of Ni ions result in smoother surfaces [7]. Their catalytic performance is better in comparison with copper and Ni-coated copper electrodes [8].

These materials also show good stability during HER [9]. For Ni–Cu alloys, different catalytic activities towards auto-thermal reforming (ATR) of methane have been obtained depending on the synthesis method chosen [10].

Annealing is one of the methods that allows the synthesis of alloy materials [11]. The alloying degree varies with the annealing temperature [12]. The Ni–Cu system shows complete solid solubility. It means that a single phase is created over the entire composition range [13]. The segregation of Cu appears due to the large differences in the melting point of Ni and Cu [14]. In the case of Ni–Cu alloys, the observed diffusion is a grain boundary one—Cu probably segregates to the boundary [15]. However, this phenomenon is studied mostly in the case of plastic deformation instead of the electrodeposited structures [16, 17]. Based on [18], annealing for 5 h at 423 K did not cause boundary migration of Cu in nanostructured Ni. Moreover, the annealing causes an increase in the crystallite size from 20 to 114 nm [19].

It is important to note that the used substrate influences the catalytic performance of the deposited material. Ni

✉ Katarzyna Skibińska
kskib@agh.edu.pl

¹ Faculty of Non-Ferrous-Metals, AGH University of Krakow, al. Mickiewicza 30, 30-059 Krakow, Poland

² Chemistry Department, Faculty of Science, Tanta University, Tanta 31527, Egypt

³ Academic Centre for Materials and Nanotechnology, AGH University of Krakow, al. Mickiewicza 30, 30-059 Krakow, Poland

catalysts show different activity towards dry reforming of methane to produce H_2 depending on the used ceramic oxide substrates [20]. The synthesis of Ni cones using the one-step method has already been well-described in the literature. To fabricate conically shaped materials, the crystal modifier [21], called also capping agent [22], is added to the electrolyte. It is believed that the growth is driven by screw dislocations [23]. Nickel ions deposit on the defected sites formed due to the presence of the screw dislocations [24]. Therefore, the parallel direction of growth is blocked, and the perpendicular one is promoted. At the beginning, Ni cones with the screw dislocations in different directions appear, then all screw dislocations have the same direction [25]. This method does not require using of any template because the anisotropy appears due to the growth kinetic differences along different crystallographic directions [26]. Then, the single electrodeposition process is enough to obtain conical structures. Due to this fact, this technique is called “one-step”. NH_4Cl is a commonly used crystal modifier. Literature review shows that the addition of this chemical component helps in the fabrication of smaller, more regular, shar-ended cones compared with the typical chloride baths [27]. Moreover, the boric acid usually added to the electrolyte, creates the complexes with the metal ions [28]. Anyway, are many synthesis parameters that can influence the morphology of the electrodeposited structures, e.g. time of the deposition, amount of the added capping agent, or applied current density [29]. The magnetic field applied during the fabrication process also influences the properties of cones [30]. Furthermore, Ni cones and other porous nanostructures can be decorated, e.g. with Rh [31] or Pd [32], using the galvanic displacement method. However, this approach is limited to the use of expensive noble metals.

This work presents a detailed characterization of Ni–Cu structures. The novelty of this work relates to the use of Ni cones as a substrate for further deposition of a thin layer of Cu. Samples were also annealed in an ambient atmosphere to allow copper to diffuse from the surface into the interior of the cones. Shifts in catalytic activity were analyzed considering changes in the chemical composition and morphology of the coatings. The results obtained provide new ideas to improve the catalytic performance of Ni structures.

2 Experimental

Nickel cones were synthesized using the one-step method. Structures were electrochemically deposited, for 5 min at 10 mA/cm^2 , from the electrolyte containing: $200 \text{ g/L NiCl}_2 \times 6H_2O$, 100 g/L H_3BO_3 , and 20 g/L NH_4Cl . Chemically polished Cu foil was used as a substrate. The thin layer of copper was deposited, from 0.5 M CuSO_4 in 0.5 M H_2SO_4 , on conical Ni structures for 2, 5, and 10 s at 10 mA/

cm^2 . In both cases, the Pt foil was used as a counter electrode, and the saturated calomel electrode (SCE) as a reference electrode. These depositions were performed using an SP200 BioLogic potentiostat (Seyssinet-Pariset, France).

Conical structures, before and after the deposition of Cu, were annealed in the tube furnace in the atmosphere of technical nitrogen (Air Liquide) at $300 \text{ }^\circ\text{C}$ for 120 min. The heating rate was $5 \text{ }^\circ\text{C/min}$. Coatings were cooled to room temperature with the furnace.

To characterize the morphology of cones after the deposition and further annealing process, photos of structures were taken using a Scanning Electron Microscope SEM JEOL-6000 Plus (Tokyo, Japan). All the specimens were 45° tilted during the observations. The chemical composition was determined using an Energy Dispersive X-ray Spectrometer (EDS).

The X-ray Photoelectron Spectroscopy XPS analyses were carried out in a PHI VersaProbeII Scanning XPS system using monochromatic $Al K\alpha$ (1486.6 eV) X-rays focused to a $100 \text{ }\mu\text{m}$ spot and scanned over the area of $400 \text{ }\mu\text{m} \times 400 \text{ }\mu\text{m}$. The photoelectron take-off angle was 45° and the pass energy in the analyzer was set to 46.95 eV (0.1 eV step) to obtain high energy resolution spectra for the C 1 s, O 1 s, Ni 2p, Cu 2p, and Cl 2p regions. A dual beam charge compensation with 7 eV Ar^+ ions and 1 eV electrons was used to maintain a constant sample surface potential regardless of the sample conductivity. All XPS spectra were charge referenced to the unfunctionalized, saturated carbon (C–C) C 1 s peak at 285.0 eV . The operating pressure in the analytical chamber was less than $4 \times 10^{-9} \text{ mbar}$. Deconvolution of spectra was carried out using PHI MultiPak software (v.9.9.3). Spectrum background was subtracted using the Shirley method.

Phase composition was analyzed using X-ray diffraction XRD with Rigaku MiniFlex II apparatus (Tokyo, Japan) equipped with the Cu lamp. The scan speed was $0.4^\circ/\text{min}$.

Changes in the roughness of synthesized coatings were determined using Atomic Force Microscopy (AFM) NTegra Aura NT MDT (Moscow, Russia) in a semicontact mode using an NSG03 tip.

Contact angles were measured using a high-speed camera Model:9501 with the HiBestViewer 1.0.5.1 software. A droplet of $10 \text{ }\mu\text{L}$ of deionized water was applied to the surface. Measurements were repeated 3 times for each sample. To determine the values of contact angle, the contour analysis was used in the Image J software version 1.8.0.

All electrochemical testing was performed using the SP200 BioLogic potentiostat. The geometric surface area of the samples was 2.8 cm^2 . Catalytic performance measurements were performed in a three-electrode cell using a Pt foil as the anode and a saturated calomel electrode (SCE) as the reference electrode. Synthesized coatings were used as the working electrode. Linear sweep voltammetry (LSV)

measurements were performed in 1 M NaOH solution. The applied range was from the open circuit potential (OCP) value to -1.6 V vs. SCE. The scan rate was 20 mV/s. The electrochemical active surface area (ECSA) measurements were performed in a 1 M NaOH solution. CV scans were performed at the following scan speeds: 40, 60, 80, 100, 140, and 180 mV/s. The stability of the coatings was determined by performing 50 CV scans at 250 mV/s after the LSV measurement. After this procedure, LSV was repeated and compared with the curve obtained.

3 Results and discussion

Metals and alloys synthesized by the one-step method show enhanced catalytic properties compared with bulk materials [2]. Ni cones were used as substrates for the deposition of thin Cu layers. The obtained coatings were additionally annealed at 300 °C. SEM photos taken at 45° are shown in Fig. 1.

The results obtained show that the electrochemical deposition of Cu did not affect the morphology of the substrates (Fig. 1a, c, e and g). Moreover, the applied annealing conditions did not change the Ni cones (Fig. 1a, b). This confirms that the process conditions used were correct. Temperatures higher than 300 °C can cause softening of the Cu foil used as a substrate for Ni cones. On the other hand, lower temperatures greatly increase the time required for Cu to diffuse from the surface of the cone. However, there are significant differences between Ni structures with Cu deposited before and after annealing, but their top part became more round-ended. Performed simulations show that the surface of Ni–Cu alloys becomes smoother after the annealing process [33]. Moreover, it suggests the changes in the chemical composition of cones. To confirm it, analyses using the EDS were performed. Results are listed in Table 1.

The chemical compositions determined confirm that the applied time of Cu deposition is sufficient. Cu was easily detected by the EDS method and its amount increased with time. At the same time, the content of Ni is lower. For all samples, the oxygen content after annealing is higher than before the process. This may be due to the adsorption of oxygen during the removal of the annealed samples from the furnace. However, attention was paid to their temperature—the furnace was completely cooled. The presence of Cl is a residual from the synthesis of Ni cones and comes from the NiCl₂ used. Therefore, the aim of the annealing process was the diffusion of Cu from the surface of the cone into its interior. In order to study this phenomenon, XPS analyses of coatings with deposited thin Cu layer were performed. The results are shown in Table 2 below. The focus was on changes in Ni and Cu content.

Within the experiment geometry, the information depth of analysis was about 5 nm. It allows the evaluation of the applied annealing process. Literature review shows, that during the annealing in nitrogen, highly Cu-rich regions are formed near the top surface layer [34]. This phenomenon is also observed, in this work, for the annealed Ni–Cu structures. The contents of Cu⁰, Cu⁺, and Cu²⁺ after annealing are much higher than for Ni⁰ and Ni²⁺.

The example of XPS spectra, for sample with 5 s of deposition of Cu, is shown in Fig. 2.

The Ni 2p_{3/2} spectra were fitted with seven lines [35]. First asymmetric line centered at 852.1 eV indicate the presence of metallic nickel [36] whereas lines within the energy range 854–863 eV indicate the Ni²⁺ in nickel oxide NiO and/or hydroxide or some part of NiCl₂ [37].

Cu 2p_{3/2} spectra were fitted with six components with the first line centered at 932.7 eV points out the existence of Cu⁰ or Cu⁺ oxidation state like in Cu₂O and due to the presence on some samples large shake-up structures found within the binding energy range of 940–946 eV [38] and additional high left “shoulder” on spectra evidenced with the lines centered at ~934 and ~935 eV the Cu²⁺ oxidation state can be identified [39].

The successful deposition of Cu is confirmed by XPS analysis. It is present on the surface of samples in the form of Cu⁰ or Cu⁺ and Cu²⁺. The metallic Ni is detected, which means that the deposited layers are thinner than 5 nm. In all cases, after annealing, the Ni⁰ has disappeared and Ni²⁺ is present instead. This means that Cu diffusion must have taken place and new phases were formed. The migration of the Cu atoms inwards was also predicted in [33].

Moreover, XRD measurements were performed. Examples of spectrum are shown in Fig. 3.

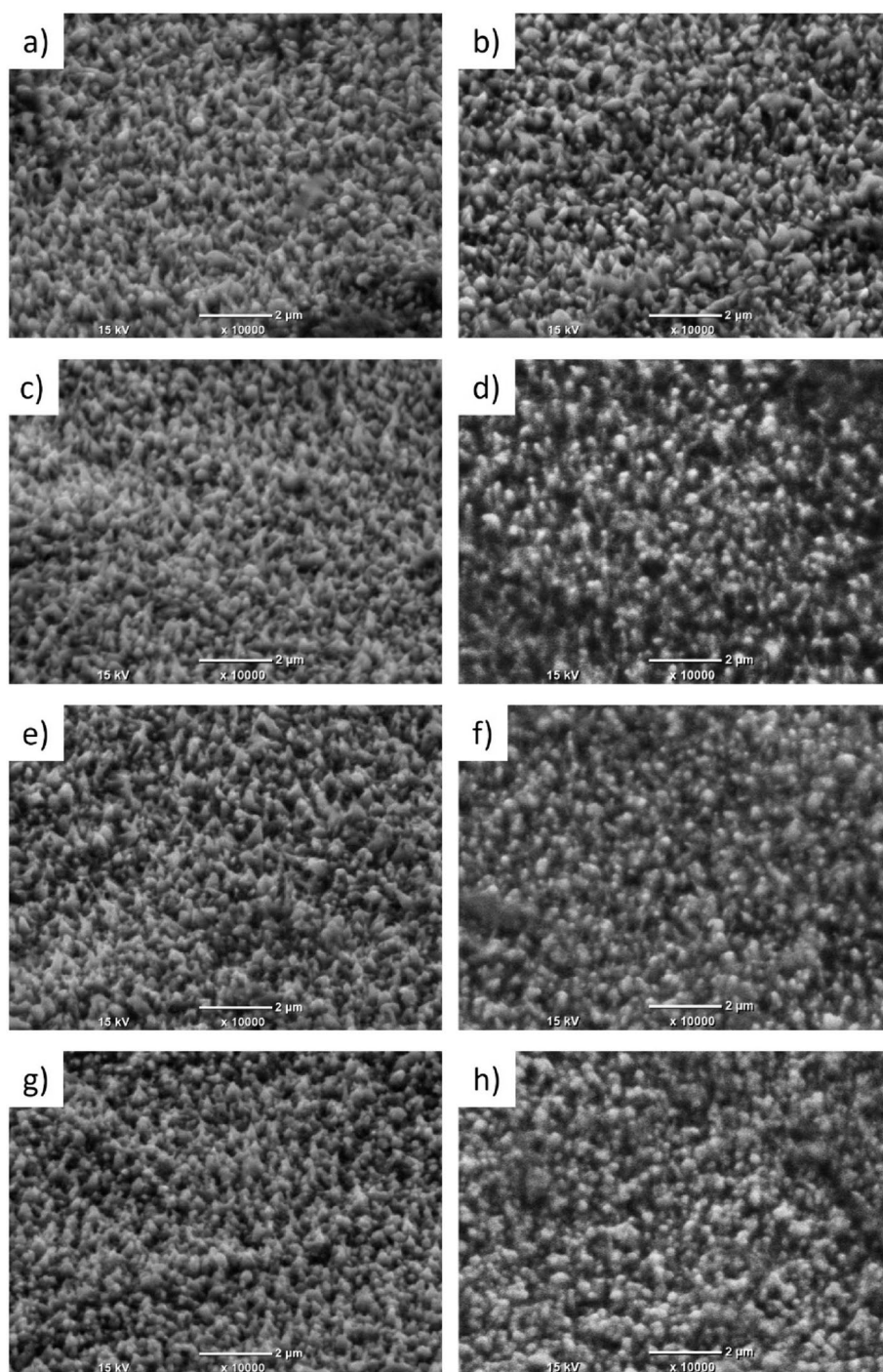
As presented, peaks coming from Ni and Cu–Ni phases cannot be distinguished directly based on obtained spectra. Peaks for Cu come from the copper foil used as the substrate for Ni cones.

As observed in SEM photos, the morphology of coatings changed after the annealing process. Changes in samples' roughness were analyzed based on AFM results. They are listed in Table 3.

For all samples, the roughness increased after the annealing process. Moreover, the deposition of Cu for 5 or 10 s increased slightly the roughness compared with the substrate—Ni cones. To the few micrometers of electrodeposition Cu, the surface is smooth which explains these small changes in roughness [40]. It can be concluded that the biggest development of the surface was obtained after annealing the sample with the layer of Cu deposited for 2 s. The examples of 3D images are shown in Fig. 4.

The provided images confirm the rounding of cones observed before in SEM photos (Fig. 1e, f).

Fig. 1 SEM photos of Ni cones after **a** 0 s, **c** 2 s, **e** 5 s, and **g** 10 s of deposition of Cu. Coatings with copper deposited for **b** 0 s, **d** 2 s, **f** 5 s, and **h** 10 s were annealed



Synthesized Ni–Cu structures could be potentially applied as catalysts in HER. One of the important factors in the reaction of hydrogen evolution is the wettability of the surface. Contact angles were measured 3 times per sample. Results are shown in Fig. 5.

The wettability of coatings increased after the annealing of Ni cones without and with the thin layer of Cu deposited for 2 and 5 s—all samples are hydrophobic. There is no change in the contact angle for the sample after 10 s of

electrodeposition. Moreover, the sample after 5 s of Cu fabrication before the annealing is characterized by a lower contact angle value than e.g. after 2 s. Even if, all samples were measured freshly after the synthesis, it seems some of them oxidized which influenced the obtained values. It relates to the affinity of Cu to oxygen.

LSV measurements were performed in 1 M NaOH. The current density was calculated assuming that the active surface area equals the geometrical surface (2.8 cm^2). The

Table 1 Chemical composition of prepared coatings

Sample	Chemical composition (% at.)			
	O	Cl	Ni	Cu
0 s	2,1	0,2	97,8	–
0 s, annealed	2,7	0,1	97,3	–
2 s	2,2	0,1	88,1	9,6
2 s, annealed	6,9	0,5	84,2	8,4
5 s	3,3	0,2	79,9	16,6
5 s, annealed	9,1	0,7	78,9	11,3
10 s	2,6	0,1	72,0	25,3
10 s, annealed	9,4	0,3	74,1	16,3

Table 2 Results of XPS analyses

Compound	Ni		Cu	
	Binding energy (eV)			
	852.1	854.3	932.7	934.0
Sample	Ni ⁰	Ni ²⁺	Cu ⁰ /Cu ⁺	Cu ²⁺
2 s	23.2	36.8	35.8	4.2
2 s, annealed	0.0	28.5	33.1	38.4
5 s	10.9	18.2	63.2	7.7
5 s, annealed	0.0	7.7	77.5	14.8
10 s	12.4	16.3	64.2	7.2
10 s, annealed	0.0	6.8	87.4	5.8

obtained curves are shown in Fig. 6. The ohmic drop determination technique, based on the impedance measurement technique (ZIR), was applied before the LSV measurement. Therefore, the IR can be determined and compensated.

According to the data presented in Fig. 6, even five seconds or more of Cu deposition increased the catalytic activity of the structures as compared to Ni cones. The small cathodic peak, especially visible for the sample after 10 s of electrodeposition, is related to the reduction of Cu oxides on the surface [41]. However, it is this coating that shows the best catalytic activity. It should be noted that the annealing of Ni cones with Cu decreases the catalytic performance of the samples—the slope of the curves and the values of the current densities achieved are smaller.

Values of E_{ONSET} so the potential at which the hydrogen evolution reaction started was determined based on curves in Fig. 6. To establish it, two tangents were plotted on the curve of the potential dependence on the current density. The point of their intersection indicates the onset potential. They are listed in Table 4.

In the case of Ni cones, annealing fastened the initial of the hydrogen evolution. However, for samples with the deposited layer of Cu, the commencement of this phenomenon was delayed. It can relate to changes in morphology as well as the wettability of the coatings' surface.

In addition, the values of the Tafel slopes were determined on the basis of the LSV curves, as shown in Fig. 7. The value of the slope of the Tafel curve, which is an indicator of the mechanism of the hydrogen evolution process, can be modified by changing the electrode material, modifying its chemical composition, phase composition, or surface development. The most desirable material is one that is characterized by low overpotential and high exchange currents.

In Fig. 7, a representation of the polarization scan with a logarithmic scale, which was used for Tafel slope determination, is shown. The low current range—lower than 1 mA/cm² is related to the charging of the double-layer and surface-dependent processes like reduction of oxidated species and adsorption/desorption of molecules. The second current range, located between 1 and 10 mA/cm² can be directly associated with the hydrogen evolution reaction. The linear course in this range can be used for the Tafel slope determination, which is commonly used in terms of mechanism identification. In the presented results, a significant difference in the Tafel slope value from 274 to 106 mV for the sample after the annealing process can be distinguished. Based on the theoretical values, the sample before the annealing process exhibited a significantly higher Tafel slope, which can be attributed to the highly inhibited mechanism of hydrogen evolution. This can be related to the formation of high-stability bonds between the electrode surface and adsorbed proton, which require significantly higher energy for recombination and H₂ formation. Surface treatment performed by annealing provides changes in the phase composition, morphology, and composition of the surface, increasing the number of electroactive spots on the electrode, where hydrogen evolution reaction is going with lower overpotential.

Below there is Table 5 with listed Tafel slope values before and after annealing process.

As can be noticed, all samples after annealing show lower Tafel slope and, therefore, highly inhibited mechanism of hydrogen evolution.

The values Tafel slope of the structures produced in this work were compared with the data found in the literature (Table 6).

After the deposition of Cu on Ni cones, as confirmed by XPS results (Table 2), Ni⁰ and Ni²⁺ and the mixture of Cu⁰, Cu⁺, and Cu²⁺ were present on the surface of Ni cones. Cu passivates in alkaline media [47]. Therefore, the deposited Cu blocked the active sites on Ni cones, and therefore, decreased its catalytic activity. These structures show much worse values of Tafel slopes. The annealing process caused the formation of Ni–Cu structures. They show improved catalytic properties compared with the literature data for Ni–Cu alloys. The values of the Tafel slope are lower. The applied annealing process caused the movement of Cu atoms

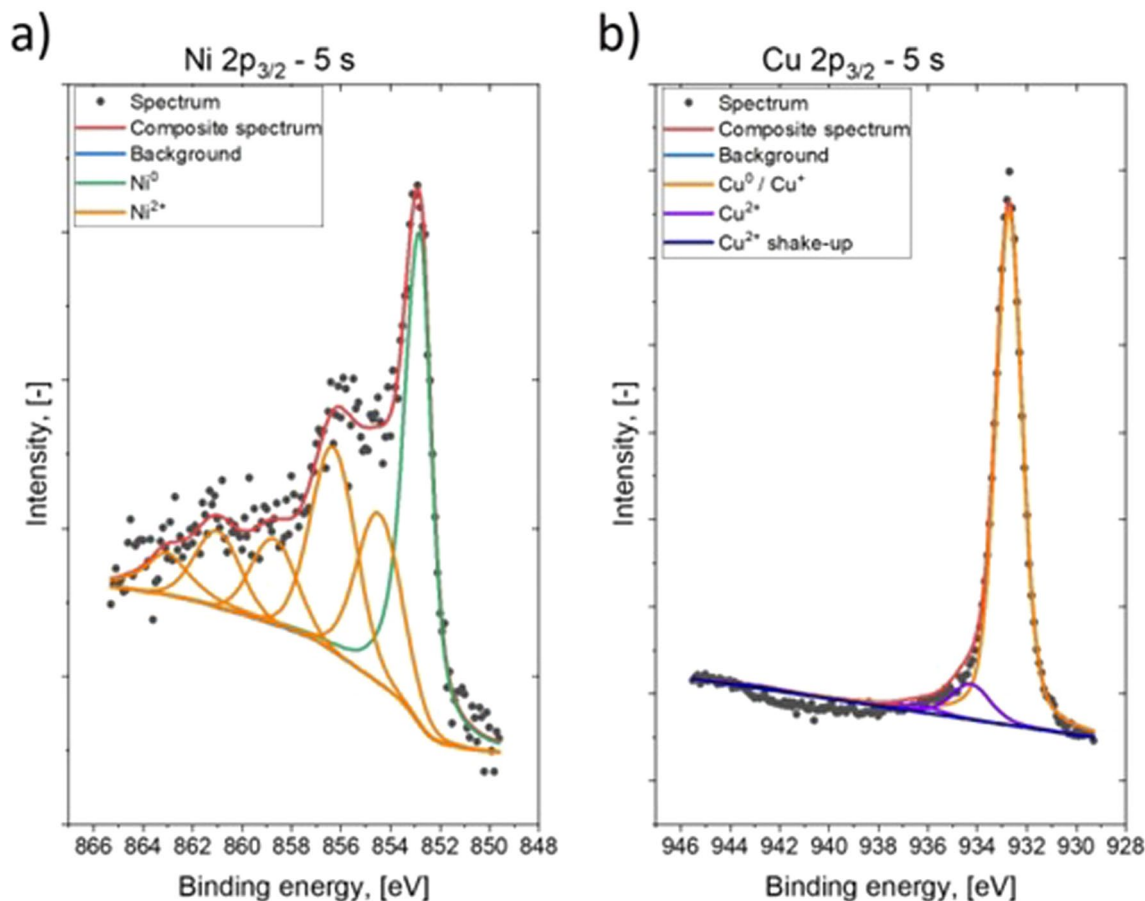


Fig. 2 Examples of a Ni 2p_{3/2} and b Cu 2p_{3/2} spectra for the sample after 5 s of Cu deposition

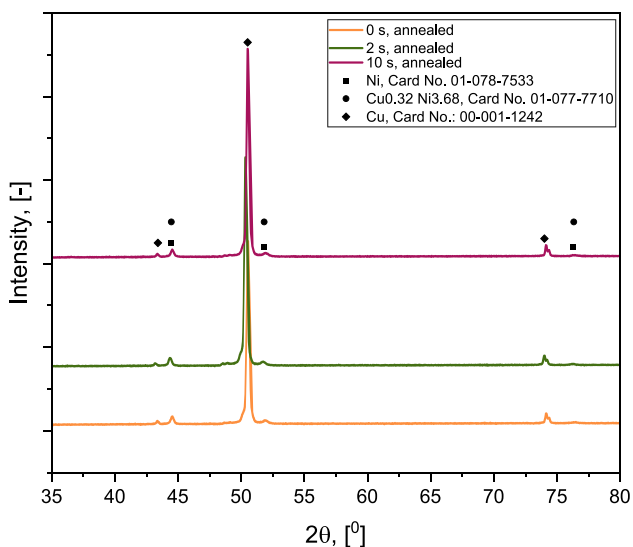


Fig. 3 XRD spectra of the annealed samples with different times of Cu deposition

Table 3 Values of coatings' roughness

Sample	Roughness (nm)
0 s	75.3
0 s, annealed	120.7
2 s	72.3
2 s, annealed	135.4
5 s	91.7
5 s, annealed	103.5
10 s	93.1
10 s, annealed	101.0

inwards Ni cones, and the creation of Ni–Cu structures, characterized by good catalytic activity.

Active surface area is a crucial factor in HER. In this work, the determination of ECSA was based on registered changes in the double-layer capacity (CDL) with the CV scan rates [48]. In a chosen range of potential, the only registered currents relate to the loading of the double-layer. The dependency between the charging currents and scan rates for the layer after 2 s of Cu deposition is shown in Fig. 8.

Fig. 4 AFM 3D image of the sample with Cu deposited for 5 s **a** before and **b** after annealing

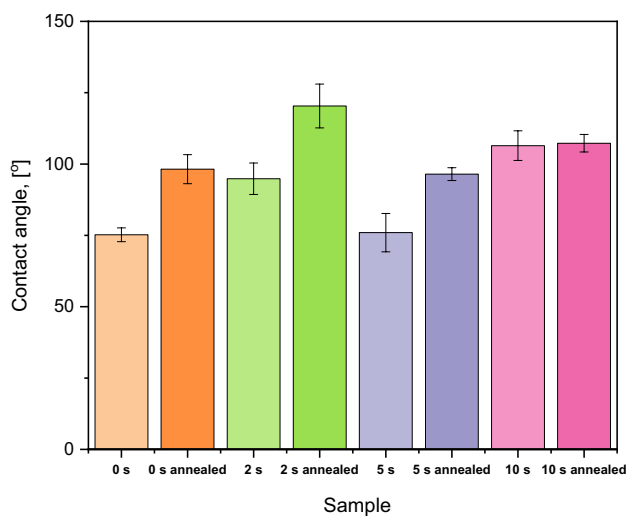
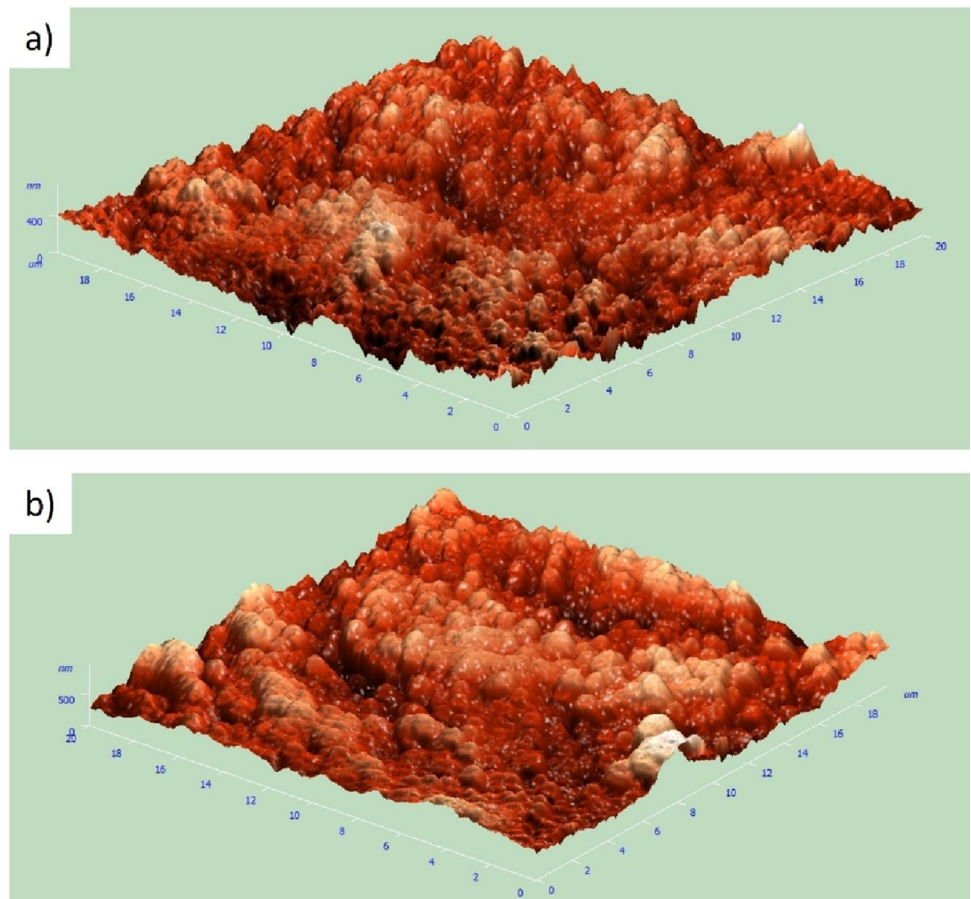


Fig. 5 Differences in the wettability between samples with deposited Cu before and after the annealing process

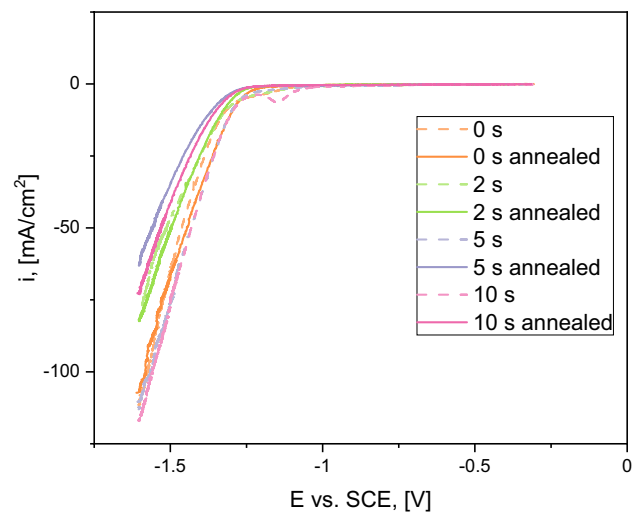


Fig. 6 Obtained LSV curves. The 85% IR-drop compensate was applied for all curves

Obtained results were compared with the value of the electrochemical active surface area for the substrate—Ni cones (11.7 cm²). Values of the S factor are listed in Table 7. It was determined from the following formula:

$$S = \frac{ECSA}{ECSA_{Ni}}, \quad (1).$$

where:

Table 4 Values of E_{ONSET}

Sample	E_{ONSET} (V)
0 s	-1.33
0 s, annealed	-1.29
2 s	-1.30
2 s, annealed	-1.31
5 s	-1.29
5 s, annealed	-1.35
10 s	-1.29
10 s, annealed	-1.35

Table 6 Literature review of Tafel slopes of Ni, Cu, and Ni–Cu alloys

Material	Tafel slope (mV/dec)	References
Pure Ni net	127	[42]
Raney-Ni	122	[42]
Ni thin film	118	[43]
Rh-decorated Ni cones	77	[31]
Cu wires	127	[44]
Ni–Cu alloys	138–181	[45]
	142	[9]
Ni–Cu nanosheets	60–80	[44]
Cu/Ni hierarchical structure	121	[46]

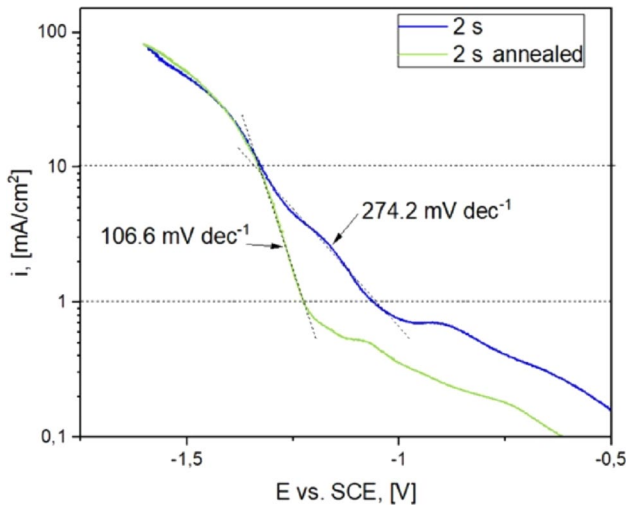


Fig. 7 Determination of Tafel slope

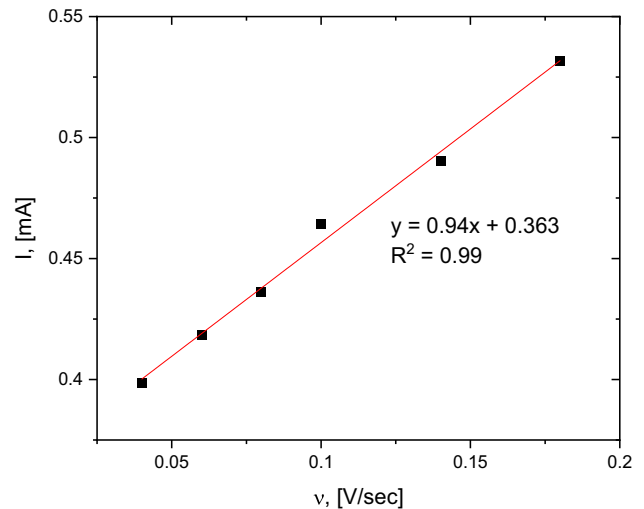


Fig. 8 Dependency between the charging currents and scan rates

Table 5 Values of Tafel slope

Sample	Tafel slope (mV/dec)
0 s	226.7
0 s, annealed	113.3
2 s	274.2
2 s, annealed	106.6
5 s	242.5
5 s, annealed	121.2
10 s	132.9
10 s, annealed	121.4

Table 7 Values of S factor

Sample	S (cm^2/cm^2)
0 s, annealed	1.3
2 s	2.0
2 s, annealed	0.4
5 s	6.7
5 s, annealed	0.7
10 s	22.0
10 s, annealed	1.6

ECSA—active surface area determined for the sample (cm^2),

ECSA_{Ni} —active surface area determined for the conical Ni substrate (cm^2).

Based on the results obtained, the active surface area of the cones with Cu decreased after annealing. In particular, for 2 and 5 s of copper deposition, the values are smaller than those of the substrate. In the case of Ni cones, the annealing process increased the determined area. The

greatest increase in active surface area was obtained after 10 s of Cu deposition. The same sample shows the best catalytic activity. However, the values obtained are approximate and cannot be used directly. The obtained trend is also opposite to that observed for the results of the AFM method, where the roughness increased after the annealing process (Table 3). The problem of a clear definition of the surface is already known from the literature [49].

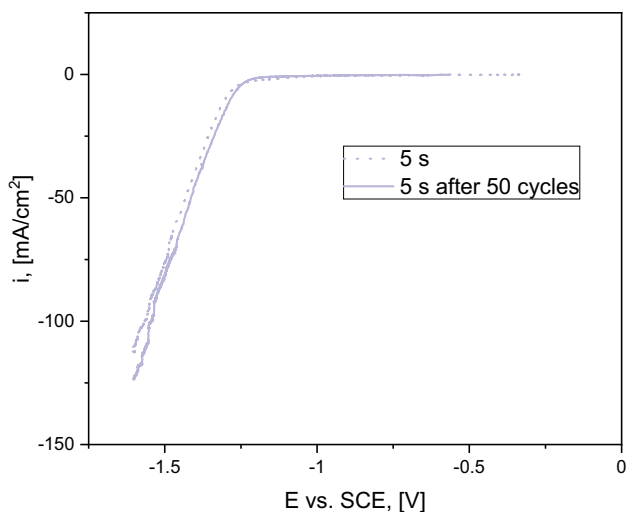


Fig. 9 LSV curves before and after 50 CV scans

In addition, the stability of the coatings was tested by repeating the CV scan 50 times. The example of LSV curves before and after 50 scans is shown in Fig. 9. The electrochemical performance for the first and 50th scans is very similar, reaching the maximum current density in the range of -120 – 125 mA/cm^2 . In terms of the Tafel slope value, there is no visible change in the mechanism of hydrogen evolution.

Obtained curves confirm the stability of Ni cones with the deposited Cu thin layer. It confirms that the synthesized structures are suitable for the application as catalysts.

4 Conclusions

All the experiments performed confirm that it is possible to obtain Ni–Cu structures using Ni cones as substrate. Five or more seconds of Cu deposition allow to increase in the catalytic performance of the structures compared to Ni cones. The synthesized material shows stability of its properties. The annealing process allowed the diffusion of Cu inside the Ni cones and consequently the formation of Ni–Cu structures. After this thermal process, the structures are rounder. The roughness of Cu coatings is increased. They are also more hydrophobic. Based on LSV measurements, the catalytic activity was degraded after the annealing process. This is due to changes in the morphology and chemical composition of the surface. Due to the higher wettability, larger bubbles should have detached from the sample surface and temporarily blocked the electrode surface. The electrochemically active surface area also changed due to the rounding of the annealed structures. However, there is no clear trend. On the other hand, the alloyed samples show better values of the Tafel slope. Nevertheless, the idea of depositing material on

Ni cones and further annealing them could be successfully applied to other metals and alloys in the future to improve catalytic or other desirable properties.

Acknowledgements This study was funded by the Polish National Science Centre (NCN), with grant number UMO-2022/45/N/ST5/00226.

Data Availability Authors can confirm that all relevant data are included in the article. Data is available in Skibińska, Katarzyna; Elsharkawy, Safya; Żabiński, Piotr, 2024, “Electrocatalytic properties of Ni–Cu structures fabricated by electrodeposition of Cu on Ni cones”, <https://doi.org/10.58032/AGH/OLAKAH>, AGH University of Krakow.

Declarations

Conflict of interest Katarzyna Skibińska declares that she has no conflict of interest. Safya Elsharkawy declares that she has no conflict of interest. Bożena Boryczko declares that she has no conflict of interest. Mateusz M. Marzec declares that he has no conflict of interest. Piotr Żabiński declares that he has no conflict of interest.

Ethical approval This article does not contain any studies with human participants performed by any of the authors.

Open Access This article is licensed under a Creative Commons Attribution 4.0 International License, which permits use, sharing, adaptation, distribution and reproduction in any medium or format, as long as you give appropriate credit to the original author(s) and the source, provide a link to the Creative Commons licence, and indicate if changes were made. The images or other third party material in this article are included in the article’s Creative Commons licence, unless indicated otherwise in a credit line to the material. If material is not included in the article’s Creative Commons licence and your intended use is not permitted by statutory regulation or exceeds the permitted use, you will need to obtain permission directly from the copyright holder. To view a copy of this licence, visit <http://creativecommons.org/licenses/by/4.0/>.

References

1. Ali N, Bilal M, Khan A, Ali F, Khan H, Khan HA, Iqbal HMN. Fabrication strategies for functionalized nanomaterials. In: *Nanomaterials: synthesis, characterization, hazards and safety*. Elsevier; 2021. pp. 55–95. <https://doi.org/10.1016/B978-0-12-823823-3.00010-0>.
2. Skibińska K, Kolczyk-Siedlecka K, Kutyla D, Jedraczka A, Leszczyńska-Madej B, Marzec MM, Zabinski P. Electrocatalytic properties of Co nanoconical structured electrodes produced by a one-step or two-step method. *Catalysts*. 2021;11:544. <https://doi.org/10.3390/catal11050544>.
3. Zabinski PR, Meguro S, Asami K, Hashimoto K. Electrodeposited Co–Ni–Fe–C alloys for hydrogen evolution in a hot 8 $\text{kmol}\cdot\text{m}^{-3}$ NaOH. *Mater Trans*. 2006;47:2860–6. <https://doi.org/10.2320/matertrans.47.2860>.
4. Zabiński PR, Franczak A, Kowalik R. Electrocatalytically active Ni–Re binary alloys electrodeposited with superimposed magnetic field. *Arch Metall Mater*. 2012;57:495–501. <https://doi.org/10.2478/v10172-012-0051-2>.
5. Chu S, Chen W, Chen G, Huang J, Zhang R, Song C, Wang X, Li C, Ostrikov K. Holey Ni–Cu phosphide nanosheets as a highly efficient and stable electrocatalyst for hydrogen evolution. *Appl*

- Catal B Environ. 2019;243:537–45. <https://doi.org/10.1016/j.apcatb.2018.10.063>.
6. Sarac U, Öksüzöğlü RM, Baykul MC. Deposition potential dependence of composition, microstructure, and surface morphology of electrodeposited Ni–Cu alloy films. *J Mater Sci Mater Electron*. 2012;23:2110–6. <https://doi.org/10.1007/s10854-012-0709-6>.
 7. Goranova D, Avdeev G, Rashkov R. Electrodeposition and characterization of Ni–Cu alloys. *Surf Coat Technol*. 2014;240:204–10. <https://doi.org/10.1016/j.surfcoat.2013.12.014>.
 8. Solmaz R, Döner A, Kardaş G. Electrochemical deposition and characterization of NiCu coatings as cathode materials for hydrogen evolution reaction. *Electrochem Commun*. 2008;10:1909–11. <https://doi.org/10.1016/j.elecom.2008.10.011>.
 9. Solmaz R, Döner A, Kardaş G. The stability of hydrogen evolution activity and corrosion behavior of NiCu coatings with long-term electrolysis in alkaline solution. *Int J Hydrogen Energy*. 2009;34:2089–94. <https://doi.org/10.1016/j.ijhydene.2009.01.007>.
 10. Lo Faro M, Frontera P, Antonucci P, Aricò AS. Ni–Cu based catalysts prepared by two different methods and their catalytic activity toward the ATR of methane. *Chem Eng Res Des*. 2015;93:269–77. <https://doi.org/10.1016/j.cherd.2014.05.014>.
 11. He S, Liu Y, Zhan H, Guan L. Direct thermal annealing synthesis of ordered Pt alloy nanoparticles coated with a thin N-doped carbon shell for the oxygen reduction reaction. *ACS Catal*. 2021;11:9355–65. <https://doi.org/10.1021/acscatal.1c02434>.
 12. Zeng W-J, Tong L, Liu J, Liang H-W. Annealing-temperature-dependent relation between alloying degree, particle size, and fuel cell performance of PtCo catalysts. *J Electroanal Chem*. 2022;922:116728. <https://doi.org/10.1016/j.jelechem.2022.116728>.
 13. DuPont JN, Lippold JC, Kiser SD. Alloying additions, phase diagrams, and phase stability. In: *Welding metallurgy and weldability of nickel-base alloy*. Wiley; 2009. pp. 15–45. <https://doi.org/10.1002/9780470500262.ch2>.
 14. Balakrishna Bhat T, Arunachalam VS. Strengthening mechanisms in alloys: a review. *Proc Indian Acad Sci Sect C Eng Sci*. 1980;3:275–96. <https://doi.org/10.1007/BF02842915>.
 15. Foiles SM. Calculation of grain-boundary segregation in Ni–Cu alloys. *Phys Rev B*. 1989;40:11502–6. <https://doi.org/10.1103/PhysRevB.40.11502>.
 16. Divinski S, Ribbe J, Schmitz G, Herzig C. Grain boundary diffusion and segregation of Ni in Cu. *Acta Mater*. 2007;55:3337–46. <https://doi.org/10.1016/j.actamat.2007.01.032>.
 17. Emeis F, Peterlechner M, Divinski SV, Wilde G. Grain boundary engineering parameters for ultrafine grained microstructures: proof of principles by a systematic composition variation in the Cu–Ni system. *Acta Mater*. 2018;150:262–72. <https://doi.org/10.1016/j.actamat.2018.02.054>.
 18. Kolobov YR, Grabovetskaya GP, Ivanov MB, Zhilyaev AP, Valiev RZ. Grain boundary diffusion characteristics of nanostructured nickel. *Scr Mater*. 2001;44:873–8. [https://doi.org/10.1016/S1359-6462\(00\)00699-0](https://doi.org/10.1016/S1359-6462(00)00699-0).
 19. Baskaran I, Sankara Narayanan TSN, Stephen A. Pulsed electrodeposition of nanocrystalline Cu–Ni alloy films and evaluation of their characteristic properties. *Mater Lett*. 2006;60:1990–5. <https://doi.org/10.1016/j.matlet.2005.12.065>.
 20. Barroso-Quiroga MM, Castro-Luna AE. Catalytic activity and effect of modifiers on Ni-based catalysts for the dry reforming of methane. *Int J Hydrogen Energy*. 2010;35:6052–6. <https://doi.org/10.1016/j.ijhydene.2009.12.073>.
 21. Liu J, Fang X, Zhu C, Xing X, Cui G, Li Z. Fabrication of superhydrophobic coatings for corrosion protection by electrodeposition: a comprehensive review. *Colloids Surf A Physicochem Eng Asp*. 2020;607:125498. <https://doi.org/10.1016/j.colsurfa.2020.125498>.
 22. Lee JM, Jung KK, Lee SH, Ko JS. One-step fabrication of nickel nanocones by electrodeposition using $\text{CaCl}_2 \cdot 2\text{H}_2\text{O}$ as capping reagent. *Appl Surf Sci*. 2016;369:163–9. <https://doi.org/10.1016/j.apsusc.2016.02.006>.
 23. Barati Darband G, Aliofkhaezrai M, Sabour A. Nickel nanocones as efficient and stable catalyst for electrochemical hydrogen evolution reaction. *Int J Hydrogen Energy*. 2017;42:14560–5. <https://doi.org/10.1016/j.ijhydene.2017.04.120>.
 24. Jin S, Bierman MJ, Morin SA. A new twist on nanowire formation: screw-dislocation-driven growth of nanowires and nanotubes. *J Phys Chem Lett*. 2010;1:1472–80. <https://doi.org/10.1021/jz100288z>.
 25. Zou R, Zhou Y, Wang J, Li Y, Gu L, Wang Y. Electrochemical approach towards the controllable synthesis of nickel nanocones based on the screw dislocation. *Appl Nanosci*. 2020;10:1625–38. <https://doi.org/10.1007/s13204-019-01233-9>.
 26. Meng F, Morin SA, Forticaux A, Jin S. Screw dislocation driven growth of nanomaterials. *Acc Chem Res*. 2013;46:1616–26. <https://doi.org/10.1021/ar400003q>.
 27. Hashemzadeh M, Raeissi K, Ashrafzadeh F, Khorsand S. Effect of ammonium chloride on microstructure, super-hydrophobicity and corrosion resistance of nickel coatings. *Surf Coatings Technol*. 2015;283:318–28. <https://doi.org/10.1016/j.surfcoat.2015.11.008>.
 28. Rahimi E, Rafsanjani-Abbasi A, Imani A, Kiani Rashid AR, Hosseinpour S, Davoodi A. Synergistic effect of a crystal modifier and screw dislocation step defects on the formation mechanism of nickel micro-nanocone. *Mater Lett*. 2019;245:68–72. <https://doi.org/10.1016/j.matlet.2019.02.093>.
 29. Skibińska K, Huang M, Mutschke G, Eckert K, Włoch G, Wojnicki M, Żabiński P. On the electrodeposition of conically nano-structured nickel layers assisted by a capping agent. *J Electroanal Chem*. 2022;904:115935. <https://doi.org/10.1016/j.jelechem.2021.115935>.
 30. Huang M, Eckert K, Mutschke G. Magnetic-field-assisted electrodeposition of metal to obtain conically structured ferromagnetic layers. *Electrochim Acta*. 2021;365:137374. <https://doi.org/10.1016/j.electacta.2020.137374>.
 31. Skibińska K, Kutyla D, Yang X, Krause L, Marzec MM, Żabiński P. Rhodium-decorated nanoconical nickel electrode synthesis and characterization as an electrochemical active cathodic material for hydrogen production. *Appl Surf Sci*. 2022;592:153326. <https://doi.org/10.1016/j.apsusc.2022.153326>.
 32. Kutyla D, Nakajima K, Fukumoto M, Wojnicki M, Kołczyk-Siedlecka K. Electrocatalytic performance of ethanol oxidation on Ni and Ni/Pd surface-decorated porous structures obtained by molten salts deposition/dissolution of Al–Ni alloys. *Int J Mol Sci*. 2023;24:3836. <https://doi.org/10.3390/ijms24043836>.
 33. Pham AV, Fang TH, Tran AS, Chen TH. Effect of annealing and deposition of Cu atoms on Ni trench to interface formation and growth mechanisms of Cu coating. *Superlattices Microstruct*. 2020;139:106402. <https://doi.org/10.1016/j.spmi.2020.106402>.
 34. Tsong TT, Ng YS, McLane SB. Surface segregation of Ni–Cu alloy in nitrogen and oxygen: an atom-probe field-ion microscope study. *J Appl Phys*. 1980;51:6189–91. <https://doi.org/10.1063/1.327652>.
 35. Biesinger MC, Payne BP, Lau LWM, Gerson A, Smart RSC. X-ray photoelectron spectroscopic chemical state quantification of mixed nickel metal, oxide and hydroxide systems. *Surf Interface Anal*. 2009;41:324–32. <https://doi.org/10.1002/sia.3026>.
 36. Biesinger MC, Lau LWM, Gerson AR, Smart RSC. The role of the Auger parameter in XPS studies of nickel metal, halides and oxides. *Phys Chem Chem Phys*. 2012;14:2434. <https://doi.org/10.1039/c2cp22419d>.

37. Biesinger MC, Payne BP, Grosvenor AP, Lau LWM, Gerson AR, Smart RSC. Resolving surface chemical states in XPS analysis of first row transition metals, oxides and hydroxides: Cr, Mn, Fe, Co and Ni. *Appl Surf Sci.* 2011;257:2717–30. <https://doi.org/10.1016/J.APSUSC.2010.10.051>.
38. Healy AMSPC, Myhra S. XPS studies of planar four-coordinate copper(II) and copper(III) complexes. *Jpn J Appl Phys.* 1987;26:L1884–7.
39. Biesinger MC. Advanced analysis of copper X-ray photoelectron spectra. *Surf Interface Anal.* 2017;49:1325–34. <https://doi.org/10.1002/sia.6239>.
40. Rasmussen AA, Jensen JAD, Horsewell A, Somers MAJ. Microstructure in electrodeposited copper layers; the role of the substrate. *Electrochim Acta.* 2001;47:67–74. [https://doi.org/10.1016/S0013-4686\(01\)00583-7](https://doi.org/10.1016/S0013-4686(01)00583-7).
41. Wan Y, Zhang Y, Wang X, Wang Q. Electrochemical formation and reduction of copper oxide nanostructures in alkaline media. *Electrochem Commun.* 2013;36:99–102. <https://doi.org/10.1016/j.elecom.2013.09.026>.
42. Zhu Y, Liu T, Li L, Song S, Ding R. Nickel-based electrodes as catalysts for hydrogen evolution reaction in alkaline media. *Ionics.* 2018;24:1121–7. <https://doi.org/10.1007/s11581-017-2270-z>.
43. Elsharkawy S, Kutyla D, Zabinski P. The influence of the magnetic field on Ni thin film preparation by electrodeposition method and its electrocatalytic activity towards hydrogen evolution reaction. *Coatings.* 2023;13:1816. <https://doi.org/10.3390/coatings13101816>.
44. Gao MY, Yang C, Zhang QB, Yu YW, Hua YX, Li Y, Dong P. Electrochemical fabrication of porous Ni–Cu alloy nanosheets with high catalytic activity for hydrogen evolution. *Electrochim Acta.* 2016;215:609–16. <https://doi.org/10.1016/j.electacta.2016.08.145>.
45. Skibinska K, Elsharkawy S, Kołczyk-Siedlecka K, Kutyla D, Żabinski P. Influence of the applied external magnetic field on the deposition of Ni–Cu alloys. *Metals.* 2024;14:1–15.
46. Wang N, Hang T, Chu D, Li M. Three-dimensional hierarchical nanostructured Cu/Ni–Co coating electrode for hydrogen evolution reaction in alkaline media. *Nano Micro Lett.* 2015;7:347–52. <https://doi.org/10.1007/s40820-015-0049-1>.
47. Hamidah I, Solehudin A, Hamdani A, Hasanah L, Khairurrijal K, Kurniawan T, Mamat R, Maryanti R, Nandiyanto ABD, Hammouti B. Corrosion of copper alloys in KOH, NaOH, NaCl, and HCl electrolyte solutions and its impact to the mechanical properties. *Alex Eng J.* 2021;60:2235–43. <https://doi.org/10.1016/j.aej.2020.12.027>.
48. Skibińska K, Elsharkawy S, Kula A, Kutyla D, Żabiński P. Influence of substrate preparation on the catalytic activity of conical Ni catalysts. *Coatings.* 2023;13:2067. <https://doi.org/10.3390/coatings13122067>.
49. Skibińska K, Kornaus K, Yang X, Kutyla D, Wojnicki M, Żabiński P. One-step synthesis of the hydrophobic conical Co–Fe structures—the comparison of their active areas and electrocatalytic properties. *Electrochim Acta.* 2022;415:140127. <https://doi.org/10.1016/j.electacta.2022.140127>.

Publisher's Note Springer Nature remains neutral with regard to jurisdictional claims in published maps and institutional affiliations.